Chiral Functionalization of an Atomically Precise Noble Metal Cluster: Insights into the Origin of Chirality and Photoluminescence

Kumaranchira Ramankutty Krishnadas,* Luca Sementa, Marco Medves, Alessandro Fortunelli, Mauro Stener,* Alexandre Fürstenberg, Giovanna Longhi, and Thomas Bürgi*

ABSTRACT: We probe the origin of photoluminescence of an atomically precise noble metal cluster, $Ag_{24}Au_1(DMBT)_{18}$ (DMBT = 2,4-dimethylbenzenethiolate), and the origin of chirality in its chirally functionalized derivatives, $Ag_{24}Au_1(R/S\text{-BINAS})_x(DMBT)_{18-2x}$, with x = 1−7 (*R*/*S*-BINAS = *R*/*S*-1,1′-[binaphthalene]-2,2′-dithiol), using chiroptical spectroscopic measurements and density functional theory (DFT) calculations. Combination of chiroptical and luminescence spectroscopies to understand the nature of electronic transitions has not been applied to such molecule-like metal clusters. In order to impart chirality to the achiral $Ag_{24}Au_1(DMBT)_{18}$ cluster, the chiral ligand, *R*/*S*-BINAS, was incorporated into it. A series of clusters, $Ag_{24}Au_1(R/S\text{-BINAS})_x(DMBT)_{18-2x}$, with x = 1−7, were synthesized. We demonstrate that the low-energy electronic transitions undergo an unexpected achiral to chiral and back to achiral transition from pure $Ag_{24}Au_1(DMBT)_{18}$ to $Ag_{24}Au_1(R/S\text{-BINAS})_x(DMBT)_{18-2x}$, by increasing the number of BINAS ligands. The UV/vis, luminescence, circular dichroism, and circularly polarized luminescence spectroscopic measurements, in conjunction with DFT calculations, suggest that the photoluminescence in $Ag_{24}Au_1(DMBT)_{18}$ and its chirally functionalized derivatives originates from the transitions involving the whole $Ag_{24}Au_1S_{18}$ framework and not merely from the icosahedral $Ag_{12}Au_1$ core. These results suggest that the chiroptical signatures and photoluminescence in these cluster systems cannot be solely attributed to any one of the structural components, that is, the metal core or the protecting metal−ligand oligomeric units, but rather to their interaction and that the ligand shell plays a crucial role. Our work demonstrates that chiroptical spectroscopic techniques such as circular dichroism and circularly polarized luminescence represent useful tools to understand the nature of electronic transitions in ligand-protected metal clusters and that this approach can be utilized for gaining deeper insights into the structure−property relationships of the electronic transitions of such molecule-like clusters.

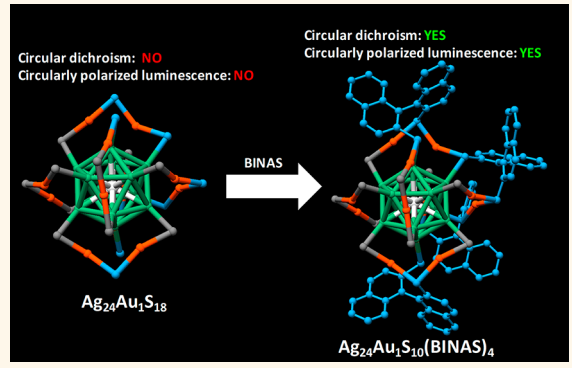

KEYWORDS: *metal clusters, chirality, circular dichroism, circularly polarized luminescence, gold clusters, alloy clusters*

Atomically precise, thiolate-protected noble metal clusters such as $Au_{102}(SR)_{44}$,[1] $Au_{25}(SR)_{18}$,[2,3] $Au_{38}(SR)_{24}$,[4−6] and $Ag_{44}(SR)_{30}$,[7−9] wherein −SR is an alkyl or aryl thiolate, are a unique class of nanoparticles[10,11] exhibiting molecule-like properties in their composition, structure, and chemical reactivity.[12] Many of these clusters consist of an inner core containing a precise number of metal atoms protected by a precise number of metal−ligand oligomeric units. For example, $Au_{25}(SR)_{18}$ consists of an inner Au_{13} icosahedron and six $Au_2(SR)_3$ units.[2,3] These clusters possess well-defined optical absorption bands which are assigned to discrete transitions between their quantized electronic energy levels.[13−15] An important manifestation of their molecule-like electronic structure is photoluminescence, which has been useful for practical applications.[16] The origin of photoluminescence and various electronic relaxation pathways of such clusters in terms of the role of their inner cores, ligands, and the metal−ligand interface has been investigated.[17−21] Processes such as ligand to metal charge transfer (LMCT) have been proposed to be at the root of luminescence in some of these

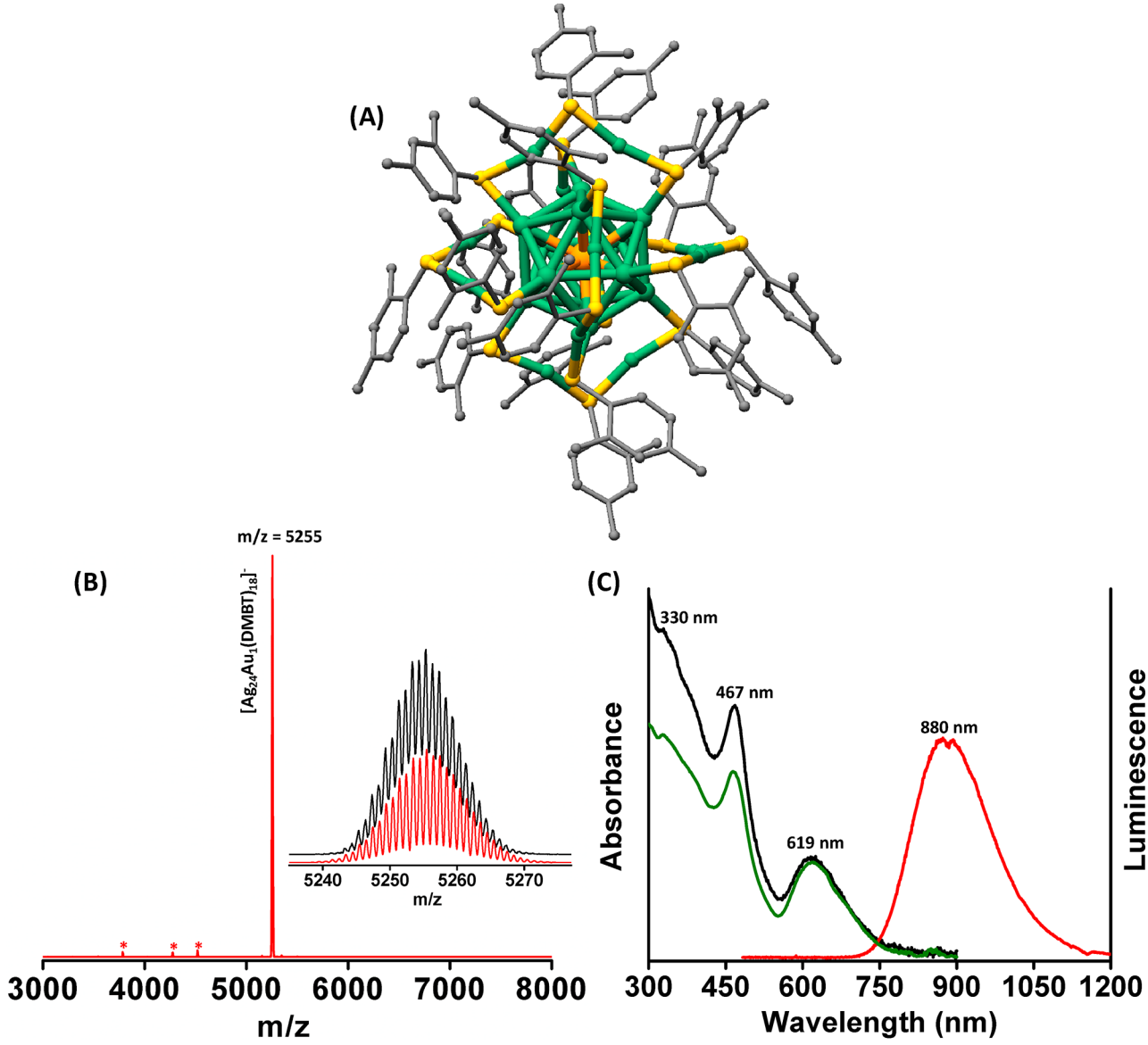

Figure 1. Schematic of the crystal structure (A), negative ion mode ESI MS spectrum (B), UV/vis absorption (black trace), excitation (green trace), and emission spectra (red trace) (C) of $Ag_{24}Au_1(DMBT)_{18}$. Inset of (B) shows the theoretical (red) and experimental (black) isotopic distribution corresponding to the formula, $Ag_{24}Au_1(DMBT)_{18}$. The features labeled with * in (B) are due to typical fragments of the molecular ion, $[Ag_{24}Au_1(DMBT)_{18}]^-$, due to sequential losses of (Ag-DMBT) units (see Figure S1). Characteristic peak positions are marked in (B) and (C). Color codes of atoms in (A): silver (green), gold (orange), sulfur (yellow), and carbon (gray). The H atoms are omitted for clarity. The structure in (A) was created using the coordinates reported in ref 18. The dip at around 880 nm in the emission spectra shown in (C) is due to an artifact from the monochromator response.

clusters.[22] Recently, Jin *et al.* showed that the metal core is mostly involved in the photoluminescence in a series of structurally related gold clusters.[23] However, in spite of being atomically precise in their compositions and possessing well-defined geometric and electronic structures, a detailed understanding of structure−property correlations of photoluminescence in these molecule-like clusters remains elusive.[23]

Circular dichroism (CD) and circularly polarized luminescence (CPL) spectroscopies are essential tools for probing the nature and the origin of the chirality in various systems. The former technique measures the difference in the absorbance of left and right circularly polarized light by a chiral molecule, whereas the latter measures the difference in the intensity of emission of left and right circularly polarized light. Therefore, these two techniques are complementary to each other, providing information about the chirality of the ground and the excited electronic (emissive) states of molecules, respectively.[24−26] In atomically precise, ligand-protected noble metal clusters, the origin of chirality has been attributed to the chirality of the ligands,[27−30] the chiral arrangement of achiral ligands on the cluster surface,[1,6] and to the inherently chiral inner metal cores.[31,32] Furthermore, discrete electronic absorption bands in some of these clusters, ($Au_{25}(SR)_{18}$, for example),[13] were assigned to the transitions involving inner cores and outer metal−ligand oligomeric units. Bearing in mind that the chirality and electronic absorption bands could be correlated with the structural features of these clusters, a combined CD and CPL investigation, in conjunction with density functional theory (DFT) calculations, is extremely helpful to unravel the origin of chiroptical signatures and photoluminescence in atomically

precise, structurally well-defined, molecule-like noble metal clusters. Such an approach, combining chiroptical and luminescence spectroscopies toward understanding the nature of electronic transitions have been used mostly for organic molecules,[33−35] and to the best of our knowledge, this method has not been applied to such molecule-like ligand-protected noble metal clusters. $Ag_{24}Au_1(DMBT)_{18}$ (DMBT = 2,4-dimethylbenzenethiolate) is an ideal system, in this regard, owing to its well-defined composition and its precisely known crystal structure.[36] Most importantly, this cluster exhibits intense photoluminescence. $Ag_{24}Au_1(DMBT)_{18}$ possesses a symmetric, achiral $Ag_{12}Au_1$ icosahedral core protected by six $Ag_2(DMBT)_3$ units and is structurally analogous to the well-known $M_{25}(SR)_{18}$ (M = Au, Ag) clusters (see Figure 1A).[36] Recent experimental investigations suggested that the photoluminescence in $Ag_{24}Au_1(DMBT)_{18}$ could be due to the charge transfer processes involving the ligands.[18] In contrast, theoretical calculations by Aikens *et al.* suggest that the photoluminescence in $M_{25}(SR)_{18}$ (M = Au, Ag) is due to the transitions involving the icosahedral core-based superatomic orbitals and that the ligand-based orbitals are not involved in these transitions.[19] Hence, the origin of photoluminescence in these clusters remains ambiguous.

Here, we investigate the origin of chiroptical signatures and photoluminescence of $Ag_{24}Au_1(DMBT)_{18}$ and its chiral derivatives using chiroptical spectroscopic measurements and DFT calculations. In order to impart chirality to the achiral $Ag_{24}Au_1(DMBT)_{18}$ cluster, a chiral ligand, *R*/*S*-1,1′-[binaphthalene]-2,2′-dithiol (*R*/*S*-BINAS) was incorporated into it. Electrospray ionization mass spectroscopic (ESI MS) measurements showed that the overall composition of the cluster remains unaltered after the incorporation of the BINAS ligand. A series of clusters, $Ag_{24}Au_1(R/S\text{-BINAS})_x(DMBT)_{18-2x}$, with x = 1−7, were synthesized. Ultraviolet/visible (UV/vis) absorption and CD spectroscopic measurements showed systematic changes in the lower-energy electronic transitions of $Ag_{24}Au_1(R/S\text{-BINAS})_x(DMBT)_{18-2x}$ as a function of the number of BINAS ligands. The CD spectroscopic measurements revealed that the incorporation of BINAS induced chiroptical signatures in the cluster and, in particular, that the low-energy electronic absorption bands undergo an unexpected achiral to chiral and back to achiral transition from pure $Ag_{24}Au_1(DMBT)_{18}$ to $Ag_{24}Au_1(R/S\text{-BINAS})_x(DMBT)_{18-2x}$ by increasing the number of incorporated BINAS ligands in them. Luminescence spectra of $Ag_{24}Au_1(R/S\text{-BINAS})_x(DMBT)_{18-2x}$ clusters are red-shifted with regard to that of $Ag_{24}Au_1(DMBT)_{18}$; furthermore, these clusters exhibit weak CPL activity, providing further insights into the nature of the excited states that are responsible for the photoluminescence. Our analysis of the trends in the UV/vis, CD, luminescence and CPL spectroscopic changes, in conjunction with DFT calculations indicates that the photoluminescence in $Ag_{24}Au_1(DMBT)_{18}$ and its chirally functionalized derivatives originate from transitions involving the whole $Ag_{24}Au_1S_{18}$ framework, not merely from the icosahedral $Ag_{12}Au_1$ core. Therefore, these results indicate that the photoluminescence in these cluster systems cannot be solely attributed to any one of the structural components, such as the metal core or the protecting metal−ligand oligomeric units. Our work also shows that, as in the case of common molecules, chiroptical spectroscopic techniques are a potential experimental tool for understanding the nature of electronic transitions in molecule-like ligand-protected metal clusters.

RESULTS AND DISCUSSION

Synthesis and Characterization of $[Ag_{24}Au_1(R/S\text{-BINAS})_x(DMBT)_{18-2x}][PPh_4]$. A schematic picture of the crystal structure of $Ag_{24}Au_1(DMBT)_{18}$ is shown in Figure 1A.[36] The negative ion mode ESI mass spectrum of $[Ag_{24}Au_1(DMBT)_{18}][PPh_4]$ (Figure 1B) shows an expected band at m/z 5255. The features labeled with * are due to typical fragments of the molecular ion, $[Ag_{24}Au_1(DMBT)_{18}]^-$, due to sequential losses of (Ag-DMBT) units, as presented in the Supporting Information (Figure S1). The theoretical and experimental isotope patterns, shown in the inset of Figure 1B, further confirm this assignment. Figure 1C shows the UV/vis absorption (black trace) and luminescence excitation (green trace) and emission (red trace) bands of $Ag_{24}Au_1(DMBT)_{18}$. Hence, the mass spectrometric and spectroscopic measurements presented above confirm the purity and the identity of this cluster.

Incorporation of the chiral ligand, *R*/*S*-BINAS, into $Ag_{24}Au_1(DMBT)_{18}$ has been carried out using the method described in the Experimental Section. Figure 2A−D shows the ESI mass spectra of the clusters obtained after the reaction of $Ag_{24}Au_1(DMBT)_{18}$ with *R*-BINAS at various $Ag_{24}Au_1(DMBT)_{18}$/BINAS molar ratios.

Figure 2A shows that the parent cluster, $Ag_{24}Au_1(DMBT)_{18}$ (see the feature corresponding to x = 0), is also present along with a series of bands, separated by 42 Da, at the higher m/z region. The mass separation of 42 Da corresponds to the loss of two DMBT ligands and incorporation of a BINAS ligand (*i.e.*, $M_{BINAS}(316) - 2 \times M_{DMBT}(2 \times 137) = 42$). Therefore, a general molecular formula, $Ag_{24}Au_1(R/S\text{-BINAS})_x(DMBT)_{18-2x}$ (x = number of BINAS ligands), is given to the BINAS-incorporated clusters synthesized. The good agreement between theoretical and experimental isotope patterns of one of the features that corresponds to x = 3 in Figure 2A, which is due to $Ag_{24}Au_1(BINAS)_3(DMBT)_{12}$ presented in Figure S2, further confirms the incorporation of the BINAS ligand into $Ag_{24}Au_1(DMBT)_{18}$. Furthermore, note that the separation between the features in the experimental isotopic pattern is 1 Da, indicating that these clusters bear single negative charge, as in the case of $[Ag_{24}Au_1(DMBT)_{18}]^-$. Figures 2A−D shows that groups of clusters containing 0−3, 2−5, 3−5, and 4−7 BINAS ligands can be synthesized by increasing the concentration of BINAS in the reaction mixture. These four groups of clusters will be referred to as groups I, II, III, and IV, respectively in the following discussion for convenience. Group IV is the mixture containing the maximum number of BINAS ligands, as shown in Figures 2D and S3D. Further increase of the concentration of the BINAS ligand did not result in the incorporation of more than seven BINAS ligands; however, clusters of different nuclearities which do not correspond to the general formula, $Ag_{24}Au_1(R\text{-BINAS})_x(DMBT)_{18-2x}$, were formed at higher concentrations of BINAS, as presented in Figure 2D. Mass spectra of the clusters synthesized with *S*-BINAS, such as $Ag_{24}Au_1(S\text{-BINAS})_x(DMBT)_{18-2x}$, at similar $Ag_{24}Au_1(DMBT)_{18}$/BINAS molar ratios are presented in Figure S3, which further confirms the incorporation of BINAS.

Note that there were no mass spectral features observed which correspond to the clusters formed by the loss of a single DMBT ligand and incorporation of a single BINAS ligand. The features corresponding to such clusters should appear at a mass separation of 179 Da (*i.e.*, $M_{BINAS}(316) - M_{DMBT}(137) = 179$); however, such features have not been detected in our measurements. Therefore, the mass spectrometric measure-

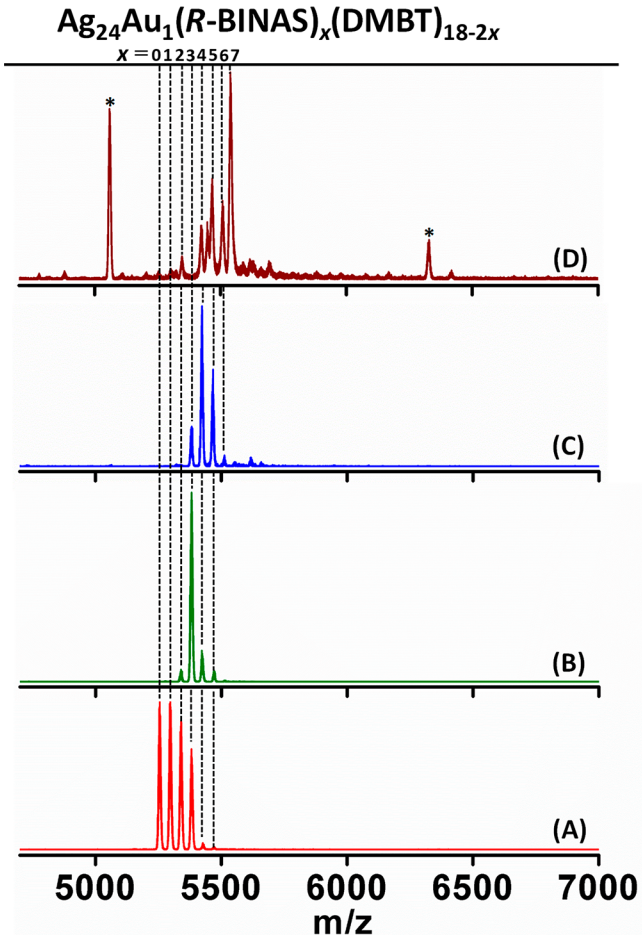

Figure 2. Negative ion mode ESI mass spectra of $Ag_{24}Au_1(R\text{-BINAS})_x(DMBT)_{18-2x}$ group of clusters I (A), II (B), III (C), and IV (D) synthesized at various $Ag_{24}Au_1(DMBT)_{18}$/BINAS molar ratios. The features (labeled with *) which do not correspond to the general formula, $Ag_{24}Au_1(R\text{-BINAS})_x(DMBT)_{18-2x}$, were also observed in (D), which could be due to decomposition or the core transformation of the $Ag_{24}Au_1(R\text{-BINAS})_x(DMBT)_{18-2x}$ resulting from the use of a slightly higher concentration of *R*-BINAS in the reaction.

ments presented above confirm that one BINAS replaces two DMBT on the clusters. It is known that the BINAS acts as a bidentate ligand to structurally analogous clusters such as $Au_{25}(SR)_{18}$ and $Au_{24}Pd(SR)_{18}$.[37,38] For example, in the case of $Au_{24}Pd(SR)_{18}$, a single BINAS binds with two Au atoms; that is, one of the two sulfur atoms of BINAS occupies the terminal position of an $Au_2(SR)_3$ staple, and the other sulfur atom occupies the bridging position of the adjacent $Au_2(SR)_3$ staple of the cluster. Considering the structural similarity of $Au_{24}Pd(SR)_{18}$, and on the basis of the mass spectrometric measurements presented above, we assume that the BINAS ligand binds to $Ag_{24}Au_1(DMBT)_{18}$ in a similar fashion. The bidentate mode of binding was further confirmed by experiments with another dithiolate ligand, namely, 1,1′-biphenyldithiol (BPT), which are presented in Figures S4 and S5. Therefore, mass spectrometric measurements unambiguously confirm the incorporation of the BINAS ligand into $Ag_{24}Au_1(DMBT)_{18}$ without altering the overall composition, that is, the total number of metal atoms and sulfur atoms and the charge state. This is surprising, considering the fact that DMBT is the only ligand known so far to protect the Ag_{25} and $Ag_{24}Au_1$ cores.

UV/Vis Absorption Measurements. UV/vis absorption spectroscopic measurements showed systematic changes in the low-energy band, at 619 nm, of $Ag_{24}Au_1(DMBT)_{18}$ as a function of the number of BINAS ligands incorporated. Figure 3 shows the UV/vis absorption spectra of groups I–IV. These measurements reveal that for I (*i.e.*, $Ag_{24}Au_1(R\text{-BINAS})_x(DMBT)_{18-2x}$ containing smaller numbers of BINAS i.e., $x = 0–3$) the spectral bands (see trace a in Figure 3) are similar to those of $Ag_{24}Au_1(DMBT)_{18}$ (see inset of Figure 3), except for some broadening of the band at around 619 nm. However, as the number of incorporated BINAS ligands increases, this band changes significantly. At higher concentration of BINAS (see traces b and c in Figure 3), $Ag_{24}Au_1(R\text{-BINAS})_x(DMBT)_{18-2x}$ exhibits a significantly broadened band with multiple features at around 590 and 664 nm, compared to the single band at around 619 nm for $Ag_{24}Au_1(DMBT)_{18}$. However, note that the shapes and the peak positions of the bands at higher energies remain almost unchanged irrespective of the number of BINAS ligands incorporated. In particular, the band at 467 nm for the $Ag_{24}Au_1(DMBT)_{18}$ is almost unchanged. However, the hump at ~380 nm and a weak shoulder at ~330 nm in parent $Ag_{24}Au_1(DMBT)_{18}$ disappeared and a weak hump/shoulder at ~362 nm appeared when BINAS was incorporated. It is interesting to note that for group IV (*i.e.*, the $Ag_{24}Au_1(R/S\text{-BINAS})_x(DMBT)_{18-2x}$ clusters containing 4–7 ligands; see mass spectra Figures 2D and S3D), a single weak absorption band, at around 590 nm, was observed in the low-energy side of the spectrum (see trace d in Figure 3) in contrast to that in groups II and III (see traces b and c in Figure 3), wherein two bands were observed. UV/vis spectra of $Ag_{24}Au_1(S\text{-BINAS})_x(DMBT)_{18-2x}$ synthesized at similar $Ag_{24}Au_1(DMBT)_{18}$/BINAS molar ratios are shown in Figure S6, which further support this trend. We observed similar changes in the UV/vis absorption bands (Figures S7 and S8) in the experiments with BPT ligand, as well. Hence, the UV/vis absorption spectroscopic measurements confirm that, as the number of dithiolate ligands on the cluster increases, the low-energy transitions are significantly altered; however, the higher energy transitions remains almost unaffected. This implies that the binaphthyl tail groups of the BINAS ligands do not significantly alter the nature of the molecular orbitals associated with higher energy transitions.

The crystal structure of $Ag_{24}Au_1(DMBT)_{18}$ shows that this cluster consists of an icosahedral $Ag_{12}Au_1$ core protected by six $Ag_2(DMBT)_3$ staple motifs,[36] which is similar to the structural framework of well-known $Au_{25}(SR)_{18}$.[2,3] Previous DFT calculations[19] suggested that the lowest-energy UV/vis absorption band of $Ag_{24}Au_1(SH)_{18}$, at around 619 nm, is due to the HOMO–LUMO electronic transition involving the superatomic orbitals derived predominantly from the metal atoms of the $Ag_{12}Au_1$ core (see however a more refined analysis below) in contrast with the charge transfer mechanism involving ligands.[18] The bands at higher energies have been assigned to transitions involving the orbitals with larger contributions from the ligands.[19] However, the clusters used in our experiments contain aromatic thiols whose interaction with the metal core is quite different with respect to the SH ligands which were used in the previous calculations. For this reason, the present calculations (see below) will furnish a different and more realistic description of the electronic structure as well as of the assignment of the most relevant optical transitions.

The incorporation of larger numbers of BINAS could lower the symmetry of the $Ag_{24}Au_1S_{18}$ framework, which might be the

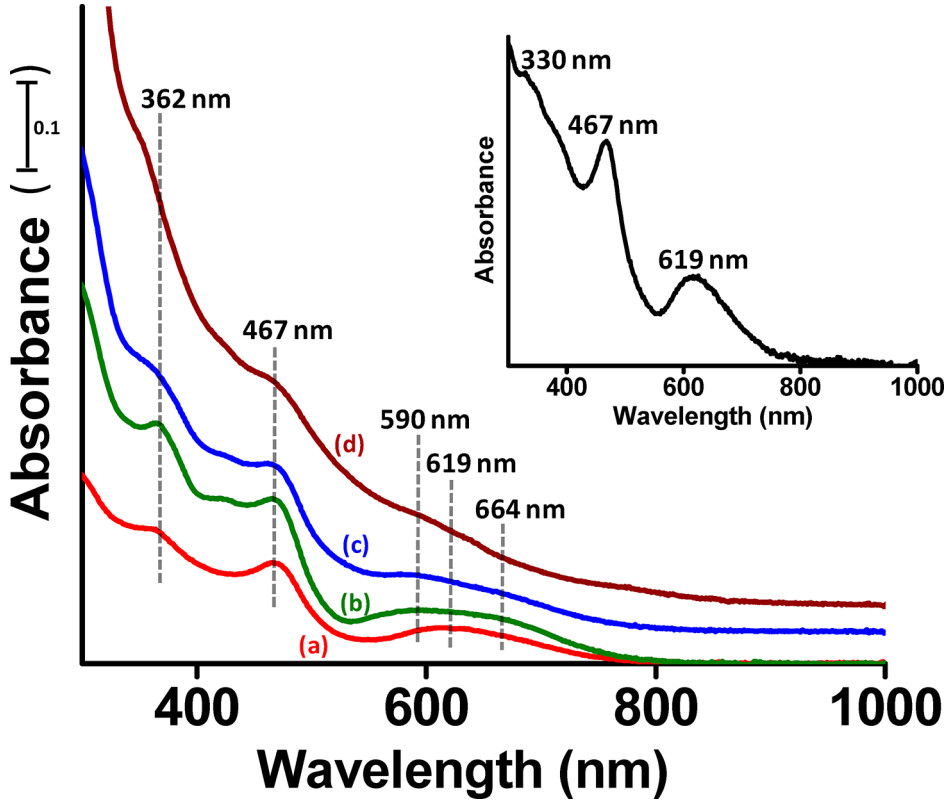

Figure 3. The UV/vis absorption spectra of $Ag_{24}Au_1(R\text{-BINAS})_x(DMBT)_{18-2x}$ group of clusters I (a), II (b), III (c), and IV (d). Inset shows the UV/vis spectrum of $Ag_{24}Au_1(DMBT)_{18}$ for comparison. Traces (b), (c) and (d) have been shifted upward for sake of clarity.

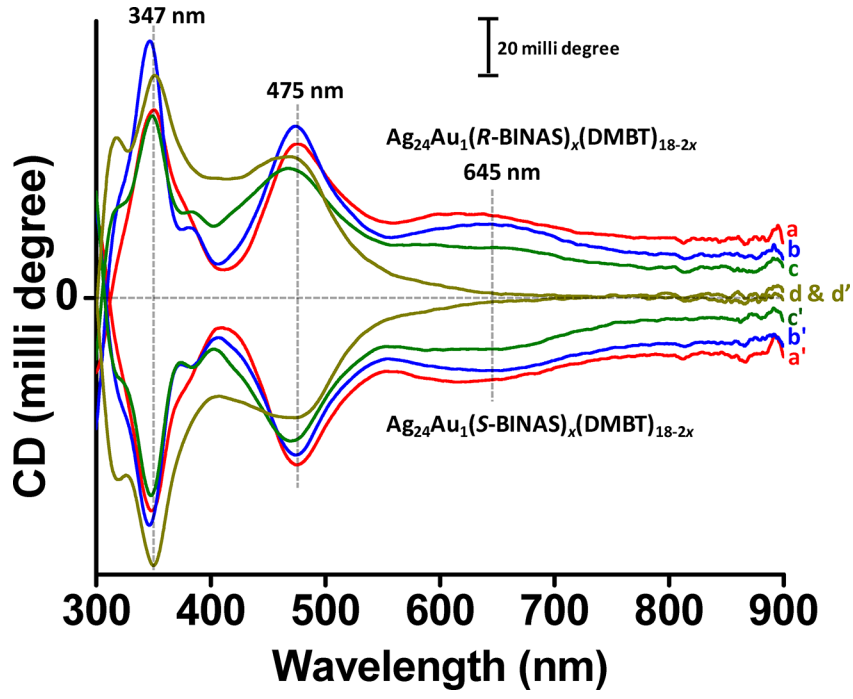

Figure 4. CD spectra of $Ag_{24}Au_1(R/S\text{-BINAS})_x(DMBT)_{18-2x}$ groups of clusters I (a and a′), II (b and b′), III (c and c′), and IV (d and d′). Traces a–d and a′–d′ correspond to the $Ag_{24}Au_1(BINAS)_x(DMBT)_{18-2x}$ clusters containing *R*- and *S*-BINAS, respectively. Traces a–c (and a′–c′) have been shifted upward (downward) for the sake of clarity.

reason for the changes in the low-energy UV/vis absorption bands. Apart from any ligand-induced structural distortions, the peak shifts and the changes in the shape of the UV/vis absorption bands can also occur due to the conjugation of the π electrons of the aromatic tail groups (*i.e.*, binaphthyl and biphenyl in BINAS and BPT, respectively). In order to test this, we attempted to incorporate aliphatic dithiols such as 1,3-propanedithiol and 1,4-butanedithiol (wherein the aromatic tail

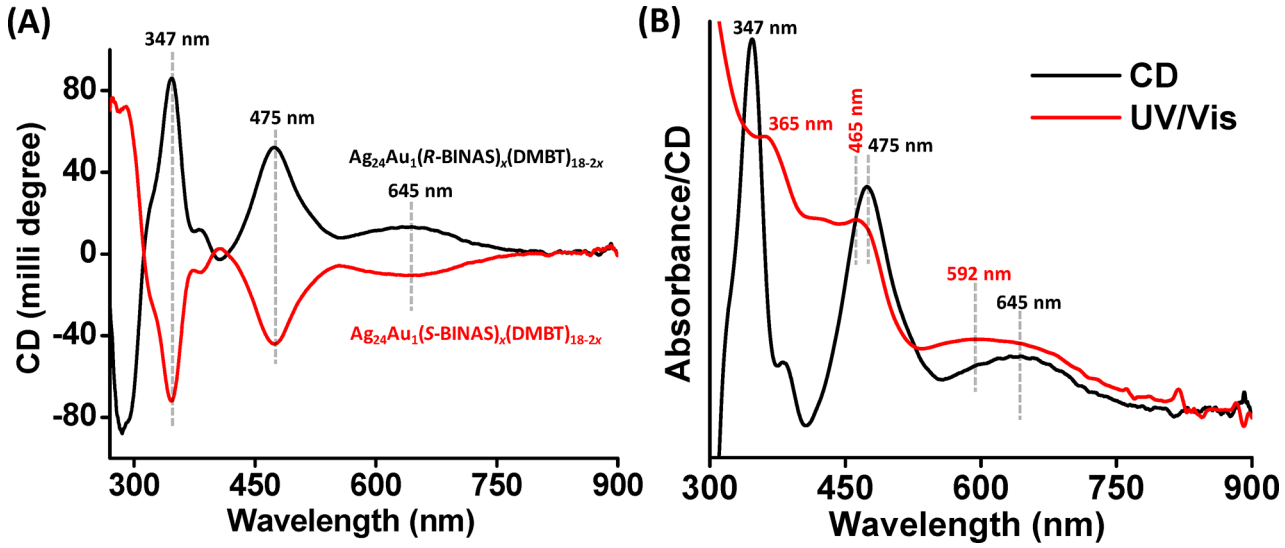

Figure 5. CD spectra (A) and a comparison of the CD and the UV/vis absorption spectra (B) of $Ag_{24}Au_1(R/S\text{-BINAS})_x(DMBT)_{18-2x}$ group II.

groups are absent); however, the reactions of $Ag_{24}Au_1(DMBT)_{18}$ clusters with these aliphatic dithiols resulted in decomposition of the cluster, and no ligand exchange was observed, in contrary to a previously reported experiment with structurally analogous $Au_{25}(SR)_{18}$.[39] Therefore, the above experiments show that the changes in the UV/vis absorption spectra of $Ag_{24}Au_1(DMBT)_{18}$ clusters induced by dithiolate ligands could be either due to structural distortions due to the bidentate binding mode or due to the conjugation of the π electrons of the ligand's tail groups. Results of the DFT calculations (see below for the details) show that structural distortions to the $Ag_{24}Au_1S_{18}$ framework indeed occur due to the incorporation of BINAS ligands.

Circular Dichroism of $Ag_{24}Au_1(R/S\text{-BINAS})_x(DMBT)_{18-2x}$: Chiral to Achiral Transition in Low-Energy Excitations. CD spectroscopy provides information about the excited electronic state manifold in relation to the ground state of a chiral molecule.[24,26] As mentioned previously, $Ag_{24}Au_1(SR)_{18}$ has a symmetric structure consisting of an icosahedral $Ag_{12}Au_1$ core and six $Ag_2(SR)_3$ staple motifs,[36] and hence, this cluster is achiral. However, in order to test whether the incorporation of the chiral dithiolate ligand, BINAS, induces any chiroptical signatures, CD measurements were carried out. The CD spectra of groups I–IV, presented in Figure 4, reveal that these clusters exhibit distinct CD bands at around 347, 475, and 645 nm with exact mirror image relationships for the clusters containing *R*-BINAS and *S*-BINAS ligands. Control experiments with pure BINAS ligand and Ag-BINAS complexes (see Figures S9 and S10) confirm that the observed CD bands are due to the dissolved clusters and not due to any impurities such as free ligands or metal–ligand complexes.

Note that group IV (see traces d and d′ in Figure 4) do not show any CD band at 645 nm, whereas groups I–III exhibit this band. The mirror image relationship is more clearly presented for group II in Figure 5A. In order to correlate the UV/vis and the CD spectral bands, a comparison of the UV/vis and CD spectra of group II is presented in Figure 5B. It is evident from Figure 5B that the strong CD band at around 475 nm coincides with the UV/vis absorption band at around 465 nm. The CD spectra of pairs of groups I, III, and IV presented separately in Figures S11–S13 further support this observation.

The band at around 467 nm in the $Ag_{24}Au_1(DMBT)_{18}$ has been assigned to the transitions involving the molecular orbitals derived from the metal atoms and ligands.[19] The coincidence of these CD and UV/vis absorption bands at 475 and 465 nm, respectively, shows that the incorporation of the chiral BINAS ligands induces chirality to the staple motifs of these clusters. Similar induction of chirality has been observed in clusters such as $Au_{25}(SR)_{18}$[37] and $Au_{38}(SR)_{24}$.[40] Furthermore, the fact that peak maxima of the bands at higher energies in UV/vis and CD spectra remain unchanged irrespective of the number of BINAS ligands incorporated indicates that the nature of the tail groups of the ligands, that is, 2,4-dimethylphenyl (in DMBT) *versus* binaphthyl (in BINAS), does not alter the net energy gaps between the molecular orbitals involved in these electronic transitions and is confirmed by present calculations (see peaks at 473–484 nm in Figure 7, left panel).

More interestingly, we observed a weak, broad CD band at around 645 nm (see Figures 4 and 5) that coincides with one of the UV/vis bands (see Figure 5B). A comparison of the UV/vis and CD traces in Figure 5B further shows that even though there are two bands at 590 and 664 nm in the UV/vis spectrum (in Figure 3), the corresponding CD spectrum shows only a single band at 645 nm. However, the CD measurements show that parent $Ag_{24}Au_1(DMBT)_{18}$, which was originally achiral, becomes chiral after functionalization with BINAS. For $Ag_{24}Au_1(R/S\text{-BINAS})_x(DMBT)_{18-2x}$ clusters containing 4–7 BINAS ligands (*i.e.*, for group IV), there are no CD bands observed at lower energies (see Figures 4 and S13) that correspond to its distinct UV/vis band at around 590 nm (see Figures 3 and S6) showing that when a large number of ligands is present the low-energy excitations lose their chiral character.

Note that even though the $Ag_{24}Au_1(R/S\text{-BINAS})_x(DMBT)_{18-2x}$ clusters with x = 4 and 5 are commonly present in groups III and IV, there is no CD band at around 600 nm for the latter. In order to understand this, we synthesized a new group of $Ag_{24}Au_1(R\text{-BINAS})_x(DMBT)_{18-2x}$ clusters with x = 3–5 (referred to as group V), wherein the cluster with x = 5 is the most abundant species. No CD band at low energies at around 645 nm was observed for group V, though there is a distinct band at around 600 nm in the UV/vis spectrum, as in the case of group IV (see Figures S14 and S15). Note that groups III and V contain clusters with the same composition although at

different relative abundances. The most abundant cluster in III is the one with $x = 4$, and that in V is the one with $x = 5$. This experiment clearly shows that this low-energy CD band in $Ag_{24}Au_1(R/S\text{-BINAS})_x(DMBT)_{18-2x}$ clusters appears only for clusters with $x = 1-4$: when $x > 4$, these clusters do not show any CD features at low energies. Therefore, the absence of this CD band at around 600 nm in groups IV and V, in spite of its presence of clusters with $x = 4$ in it, could be because of their lower concentrations in IV and V compared to that in III. A probable reason for the absence of this CD band for groups IV and V is provided below in light of the DFT calculations.

DFT Calculations on $Ag_{24}Au_1(R/S\text{-BINAS})_x(DMBT)_{18-2x}$. In order to gain better insight into the origin of the experimentally observed electronic absorption and CD bands of $Ag_{24}Au_1(R/S\text{-BINAS})_x(DMBT)_{18-2x}$ clusters, DFT calculations were performed. Note that irrespective of the $Ag_{24}Au_1(DMBT)_{18}$/BINAS molar ratios used in the synthesis, a mixture of $Ag_{24}Au_1(R/S\text{-BINAS})_x(DMBT)_{18-2x}$ clusters was formed. Furthermore, considering the structural similarity of $Ag_{24}Au_1(DMBT)_{18}$ with $Au_{25}(SR)_{18}$ and $Au_{24}Pd(SR)_{18}$,[2,3,36,38] we assume that the BINAS ligand in $Ag_{24}Au_1(R/S\text{-BINAS})_x(DMBT)_{18-2x}$ exists in a bidentate fashion, binding two adjacent $Ag_2(SR)_3$ staple motifs (see Figure 6).

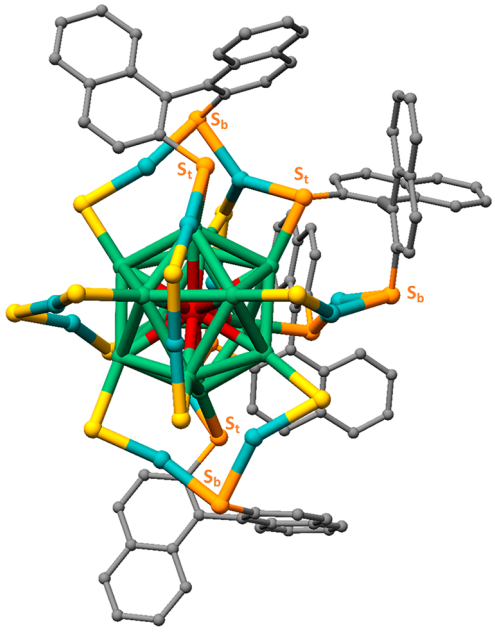

Figure 6. DFT/local density approximation fully relaxed geometry of "best 1" isomer of the $[Ag_{24}Au_1(S\text{-BINAS})_4(DMBT)_{10}]^-$. The DMBT ligands and the hydrogen atoms are omitted for clarity. Atom colors: Ag atoms in the Ag_2S_3 staples (cyan), in $Ag_{12}Au_1$ icosahedron (green), Au atom in center of the icosahedron (red), S atoms of DMBT ligands (yellow) and that of BINAS ligands (orange), carbon atoms (black). Some of the bridging and terminal S atom locations (labeled S_b and S_t, respectively) are marked to show the nature of the binding of BINAS ligands.

The introduction of the new ligand (*i.e.*, BINAS) onto $Ag_{24}Au_1(DMBT)_{18}$ generates a large number of structural isomers because there are various unique binding sites (*i.e.*, pairs of S atom locations in adjacent staples; see Figure 6) for the new ligand. For a single BINAS ligand, that is, for $Ag_{24}Au_1(R/S\text{-BINAS})_1(DMBT)_{16}$, there is only one unique binding site available, and hence, no isomers exist. However, for $x = 2$ and $x = 3$, the number of unique binding sites increases, and hence, the number of structural isomers increases to six and seven, respectively.[38] As it would be computationally very demanding to perform computations on all of the isomers of $Ag_{24}Au_1(R/S\text{-BINAS})_x(DMBT)_{18-2x}$ generated for each value of x, we focused our computational analysis on a specific composition of $Ag_{24}Au_1(R/S\text{-BINAS})_x(DMBT)_{18-2x}$, namely, the $[Ag_{24}Au_1(S\text{-BINAS})_4(DMBT)_{10}]^-$ cluster anion. The cluster, $Ag_{24}Au_1(S\text{-BINAS})_4(DMBT)_{10}$, has been chosen for simulations primarily because this cluster is present in all of the four groups (I-IV) in various abundances (although the mass spectral intensity of this cluster is low in group I, Figure 2A), and hence, it would fairly represent groups I–IV.

Structural models of $[Ag_{24}Au_1(S\text{-BINAS})_4(DMBT)_{10}]^-$ were generated as follows. Starting from the reported experimental single-crystal X-ray coordinates of the $Ag_{24}Au_1(DMBT)_{18}$ cluster anion,[36] we replaced four pairs of DMBT ligands with 4 *S*-BINAS ligands *via* a systematic docking procedure. We first identified all of the possible pairs of S atoms suitable to host a *S*-BINAS ligand on the $Ag_{24}Au_1S_{18}$ framework as those belonging to two neighboring S–Ag–S–Ag–S staples and lying at a distance not larger than a chosen cut off of 4.5 Å (of the order of the equilibrium distance between S atoms in the BINAS ligand). We then generated an ensemble of $[Ag_{24}Au_1(S\text{-BINAS})_4(DMBT)_{10}]^-$ isomers by docking the 4 *S*-BINAS ligands onto the previously identified S atom pairs and completing the rest of the ligand shell with 10 DMBT ligands. It turned out that 42 isomer structures were generated *via* this docking procedure. Note that we did not take into account the cluster symmetry in the structure generation. These structures were then subjected to local relaxations with the internal $Ag_{12}Au_1$ core kept frozen and the rest of the coordinates fully optimized. Two of the isomeric structural models thus produced were found to be almost isoenergetic and more stable than the others by few tenths of electronvolts and were, therefore, selected for further study (energies and coordinates of all isomer structural models are reported in the Table S3): hereafter, these two most stable isomers are referred to as "best 1" and "best 2" geometries. Optical absorption spectra were simulated on these final optimized geometries *via* real time time-dependent density functional theory (TDDFT) and complex polarizability algorithm[41,42] approaches.

In Figure 7, the absorption and CD spectra of $[Ag_{24}Au_1(S\text{-BINAS})_4(DMBT)_{10}]^-$ are reported, which are calculated at the TDDFT/LB94/TZV level for "best 1" and "best 2" geometries (reported in Table S4), fully optimized at the local density approximation (LDA) level. As presented previously (see Figures 3 and 4), incorporation of BINAS ligands most significantly alters the low-energy UV/vis and CD bands (i.e., 619 nm and at 632 nm, respectively) of $Ag_{24}Au_1(DMBT)_{18}$, whereas the bands at higher energies are less affected. DFT calculations also reveal a similar trend as shown in Figure 7 (left panel) when comparing $[Ag_{24}Au_1(S\text{-BINAS})_4(DMBT)_{10}]^-$ with $[Ag_{24}Au_1(DMBT)_{18}]^-$. The calculated absorption profiles of the two geometries ("best 1" and "best 2") show some differences, suggesting that structural differences between isomers play a role in photoabsorption. It is worth noting that the bands calculated at 473 nm (for "best 1") and 484 nm (for "best 2") are in nice agreement with the experimental counterpart at 467 nm (see Figure 3) and the one at 356 nm present only in "best 1", which is in nice agreement with the experimental band at 362 nm (see Figure 3). The matching between theory and experiment is less precise at low energy: the

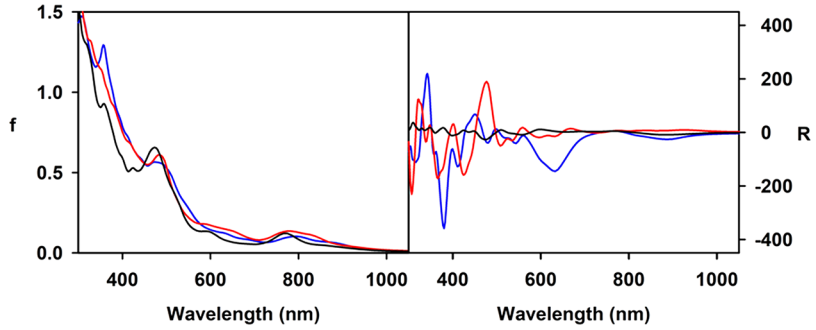

Figure 7. Photoabsorption oscillator strength (*f*, left panel) and circular dichroism rotatory strength (*R*, right panel) calculated at the TDDFT/LB94/TZV level for the geometries "best 1" (blue) and "best 2" (red) of the $[Ag_{24}Au_1(S\text{-BINAS})_4(DMBT)_{10}]^-$ cluster anion; see text for details. The spectra for the $[Ag_{24}Au_1(DMBT)_{18}]^-$ cluster anion (black lines) are also shown for comparison.

bands at 795 nm (for "best 1") and at 775 nm (for "best 2") do not have an experimental counterpart. We argue that the employed LB94 xc-potential underestimates the energy position of these bands (as it occurs with this xc-functional) that are thus missing as distinct bands in the experiment, probably hidden in the long wavelength spectral tail of the experimental bands which appear at around 619 nm. More accurate xc-functionals (such as hybrid ones), presently not implemented with the complex polarizability algorithm, on experimentally derived geometries would be needed to achieve a good agreement between theory and experiment also at low energies.[43] Interestingly, from the analysis of the CD spectra in Figure 7 (right panel), it is clear that the calculated bands at 795 and 775 nm are not detected in CD-simulated spectra; that is, they have a very low rotatory strength. Considering that the LB94 spectra are qualitatively correct in terms of spectral bands,[43] we use them as an acceptable compromise. To further support this strategy, we tried to employ the B3LYP functional[44] with the conventional Casida approach; however, due to the computational cost of the nonlocal exchange, it has been possible to extract only very few discrete excitations, so the calculated spectrum does not cover the spectral region below 500 nm. Instead, we have been able to calculate the whole photoabsorption spectrum at the B3LYP level by means of the very recent hybrid diagonal approximation approach,[45] and the results are presented in Figure S16. Interestingly, the band predicted by LB94 at around 800 nm is blue-shifted and reduced in intensity and appears as a weak shoulder (around 745 nm) of a stronger peak whose maximum lies at 653 nm. This comparison shows that the description of the low-energy part of the spectrum is improved if a hybrid xc-functional is employed, corroborating our hypothesis to ascribe the disagreement between theory and experiment at 800 nm to deficiencies of the LB94 xc-potential. Experimentally derived geometries would be needed to perfect the agreement between theory and experiment.[43] The other features at lower wavelengths are less sensitive to the choice of the xc-functional.

In contrast with photoabsorption, the TDDFT-simulated CD spectra shown in Figure 7 (right panel) are rather sensitive to the difference in geometries of "best 1" and "best 2". The comparison with experiment is not straightforward for this property; however, we can say that, at least qualitatively, most of the experimental bands are reproduced by theory in the "best 1" structure. The experimental CD profile of the *S* enantiomers of groups I–IV (Figure 4) is characterized by a broad negative minimum at 645 nm, followed by two other negative minima at 475 and 347 nm, further followed by a sudden change of sign of the CD, which becomes positive below 300 nm. In the TDDFT-simulated CD profile of "best 1", we find a broad negative minimum at 632 nm, followed by two additional minima at 480 at 380 nm and then a sudden change of sign of the CD which becomes positive below 352 nm. The comparison is rather satisfactory in terms of peak positions, albeit less quantitative in terms of intensity. The disagreement between theory and experiment may also be ascribed to the conformational degrees of freedom of the ligands, which are not accounted for in the present simulations and have important consequences on the CD intensity.[46]

It is interesting to note that the UV/vis absorption band at 795 nm in "best 1" does not have a counterpart in its calculated CD spectrum. This can be explained *via* an individual component maps of rotatory strength (ICM-RS) analysis (see ref 47). It represents the most sophisticated tool of chiroptical response and is reported for $[Ag_{24}Au_1(S\text{-BINAS})_4(DMBT)_{10}]^-$ ("best 1" configuration) in Figures S17 and S18, which shows that all three magnetic dipole contributions to the CD spectrum of "best 1" are nonzero but they nearly cancel each other to give an almost zero chiroptical response. Moreover, a molecular orbital (MO) analysis of this cluster shows that the ICM-RS plots have contributions from several different excited configurations. Table S1, reporting the analysis of the transition density matrix of the excitation at 795 nm in terms one-electron excited configurations (occupied-virtual pairs), provides more detail. The largest contribution (30%) is given by the HOMO−2 → LUMO configuration, mixed with 25% of the HOMO−1 → LUMO+1 and 11% of the HOMO−2 → LUMO+1 ones. Such excited configurations are shown as vertical arrows in Figure 8, where the MO energy levels are reported together with a Mulliken analysis of Ag, Au, S, and C+H contributions. As reported in Table S1 and in Figure 8, the occupied orbitals playing a role in the transition at 795 nm are contributed mainly by S 3p and Ag 5s atomic functions involved in the Ag–S staple chemical bonds, whereas the virtual orbitals are mainly contributed by Ag 5s. 3D plots of these molecular orbitals reported in Figure S19 confirm their nature: whereas HOMO−1 and HOMO−2 appear to be localized near the Ag–S bonds, LUMO and LUMO+1 are much more delocalized over the metal atoms, extending on the metal core, as well. This suggests that the low rotational strength at 795 nm may be due to cancellation effects among occupied virtual pairs, with the same virtual orbitals delocalized over the less chiral metallic core of the cluster, whereas chirality is mainly induced by staples.

It is interesting to investigate also the nature of the CD band calculated at 632 nm for "best 1" geometry. An analysis in terms

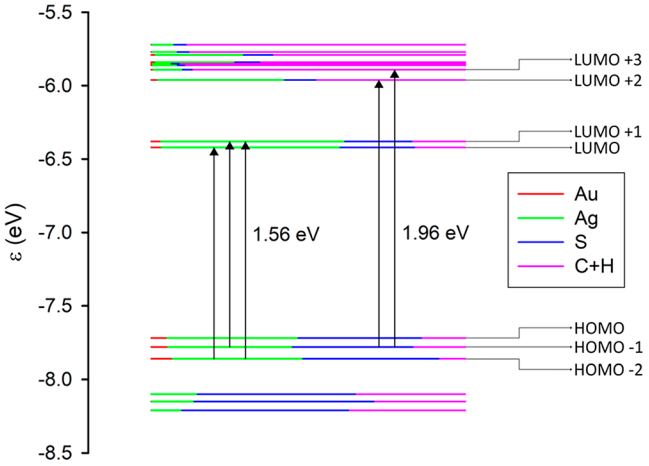

Figure 8. Molecular orbital (energy levels) diagram showing the leading contributions to the two lowest transitions at 1.56 eV (795 nm) and 1.96 eV (632 nm) for the geometry "best 1" of the $[Ag_{24}Au_1(S\text{-BINAS})_4(DMBT)_{10}]^-$ cluster anion. Orbital character in terms of Mulliken analysis of Ag, Au, S, and C+H contributions is given in terms of colors of the level, according to the inset legend. HOMO and LUMO are at −7.60 and −6.33 eV, respectively.

of excited configurations for this transition is reported in Table S1, whereas the involved orbitals are the ones reported in Figure S19. In this case, the involved virtual orbitals are LUMO+2 and LUMO+3, which contain a dominant ligand contribution (see the strong participation of the BINAS π orbitals; see Table S1 and Figure S19), while concomitantly the CD rotational strength is much more pronounced with respect to the transition calculated at 795 nm, where the ligand contribution is much smaller. This suggests that the CD signal at 632 nm in calculated spectra (see Figure 7, right panel), that we claim corresponds to the broad experimental band centered at 645 nm (see Figures 4 and 5), is generated by the asymmetry of the $Ag_{24}Au_1S_{18}$ framework induced by the ligands. For completeness, we report in Table S1 also the analysis of the features calculated for the "best 1" structure at 2.54 eV (488 nm) and 2.72 eV (356 nm), which correspond to the experimental bands at 475 and 347 nm, respectively. Unfortunately, these transitions are strongly mixed, so their assignment is not straightforward. However, from the orbitals involved, it can be seen that they are both mainly contributed by the ligands (S 3p and C 2p) with a minor contribution of the metal atoms. A more comprehensive description can be extracted from the ICM-OS plots reported in Figure S18. The strongly mixed character is corroborated by the "spots" on the reference straight line, indicating mixing of almost degenerate configurations. The minor role of the off-diagonal spots rules out plasmonic behavior, as can be expected due to the too small size of the cluster.

Further simulations on the "best 1" structure were conducted to elucidate the origin of chirality. In detail, a $[Ag_{24}Au_1(SCH_3)_{18}]^-$ model structure was generated from "best 1" geometry of the $[Ag_{24}Au_1(S\text{-BINAS})_4(DMBT)_{10}]^-$ anion by transforming its BINAS and DMBT ligands into thiomethyl residues and relaxing the geometry, first keeping the $Ag_{24}Au_1S_{18}$ core frozen and using DFT/PBE-D3 with CP2K code and then fully relaxing the resulting model using DFT/LDA with ADF code (the final structure is named "best 1-CH_3"). Any residual chiral response of this model structure must be related to a desymmetrization of the $Ag_{24}Au_1S_{18}$ framework of the parent $Ag_{24}Au_1(DMBT)_{18}^-$ induced by the replacement of DMBT with BINAS ligands, significant enough to survive as a local energy minimum even after the transformation into thiomethyl ligands. The TDDFT-simulated CD spectrum of "best 1-CH_3" is reported in Figure 9 and compared with that of

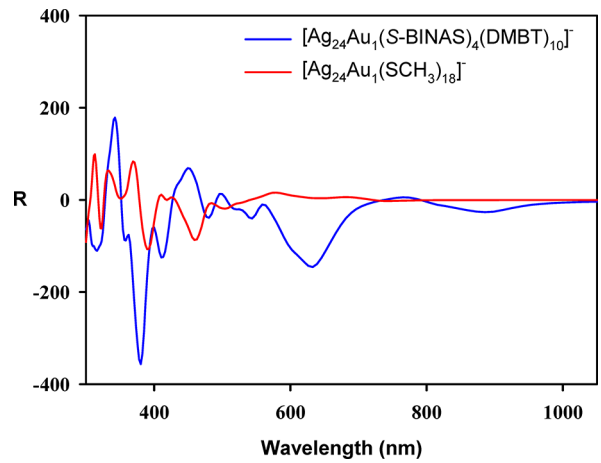

Figure 9. Circular dichroism rotatory strength (R) calculated at the TDDFT level for the $[Ag_{24}Au_1(S\text{-BINAS})_4(DMBT)_{10}]^-$ cluster anion (geometry "best 1") and a $[Ag_{24}Au_1(SCH_3)_{18}]^-$ model structure derived from the " "best 1" " by transforming the BINAS and DMBT ligands into thiomethyl residues; see text for details.

the "best 1" structure. A residual, although much damped, CD activity for "best 1-CH_3" is apparent, with values of rotator strength (R) ranging between −50 and +60. This finding suggests that the chiral desymmetrization due to the BINAS ligands partially transfers into the staple units but leaves the icosahedral metal core almost unaffected, as visualized in Figure S20, where we compare the $Ag_{24}Au_1S_{18}$ skeletons of the geometries: "best 1-CH_3" with the experimental structure of $[Ag_{24}Au_1(DMBT)_{18}]^-$. Note that the TDDFT-simulated rotatory strength of a $[Ag_{24}Au_1(DMBT)_{18}]^-$ model structure calculated following the same protocol as used for $[Ag_{24}Au_1(S\text{-BINAS})_4(DMBT)_{10}]^-$ is negligible (as shown in Figure S21), confirming the achiral nature of the starting compound. We conclude that the CD of the $[Ag_{24}Au_1(S\text{-BINAS})_4(DMBT)_{10}]^-$ at 632 nm is not directly due to chiral BINAS ligands, but the chiral ligands induce a structural lowering of the symmetry of the $Ag_{24}Au_1S_{18}$ framework, mainly in the staple units. The ligand's tail groups also contribute significantly to the intensity of these CD bands.

DFT calculations predict the presence of a CD band at 632 nm, which is assigned to the experimental band at 645 nm for groups I–III. As shown in Figure S20, the $Ag_{24}Au_1S_{18}$ skeleton of the "best 1-CH3" geometry of $Ag_{24}Au_1(S\text{-BINAS})_4(DMBT)_{10}$ exhibits structural distortions compared to that in the experimental structure of $[Ag_{24}Au_1(DMBT)_{18}]^-$. The $Ag_{24}Au_1(R/S\text{-BINAS})_x(DMBT)_{18-2x}$ clusters with x = 5–7 are more uniformly surrounded by the BINAS ligands, and the distortions by these uniformly arranged ligands could result in a more symmetric $Ag_{24}Au_1S_{18}$ skeleton compared to that in the clusters with x = 1–4 in I–III. This could result in the absence of this CD band at low energies. The absence of this band in group IV, in spite of the presence of clusters with x = 4 in it, could be because of their lower concentrations in IV compared to that in III. Although the clusters with x = 4 exhibit a CD band at 645 nm, it could be invisible due to the low concentration of these clusters compared to the other two clusters with x = 5–7 which

do not show any such CD band. Therefore, we think that the absence of the CD band at 645 nm for IV could be due to the different relative concentrations of these two different types of clusters.

Luminescence and Circularly Polarized Luminescence Measurements. Figure 10 shows the photoluminescence

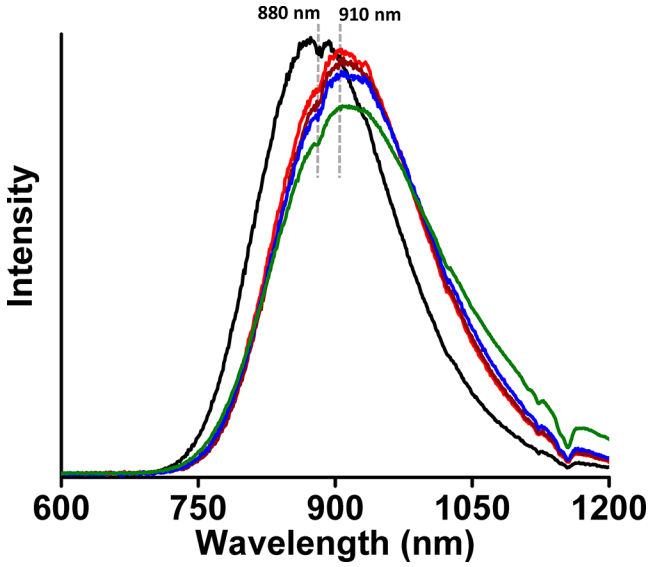

Figure 10. Luminescence spectra of $Ag_{24}Au_1(DMBT)_{18}$ (black) and $Ag_{24}Au_1(R\text{-BINAS})_x(DMBT)_{18-2x}$ group of clusters I (red), II (wine red), III (blue), and IV (green) collected at excitation wavelength of 467 nm.

spectra of $Ag_{24}Au_1(DMBT)_{18}$ and $Ag_{24}Au_1(R\text{-BINAS})_x(DMBT)_{18-2x}$ group of clusters I–IV. The excitation spectra of groups II and III are presented in Figures S22 and S23, respectively. The emission spectra of the parent $Ag_{24}Au_1(DMBT)_{18}$ and group II clusters collected at various excitation wavelengths are presented in the Figures S24 and S25, which shows that the nature of the emission band does not depend on the excitation wavelength. The emission maximum of groups I–IV undergoes a red shift of ~30 nm with regard to that of $Ag_{24}Au_1(DMBT)_{18}$. The red shift of the luminescence was further confirmed with clusters containing another bidentate ligand, namely, BPT, as presented in Figures S26 and S27.

The observed red shift in the emission bands of I–IV could either be due to the change in the ligand's tail group, that is, from 2,4-dimethylbenzyl to binaphthyl (through the extended conjugation of π electrons) or due to the structural distortion of the $Ag_{24}Au_1S_{18}$ framework due to the bidentate mode of binding, as discussed previously. DFT calculations on $Ag_{24}Au_1(S\text{-BINAS})_4(DMBT)_{10}$ reveal that there is structural distortion on the $Ag_{24}Au_1S_{18}$ framework. However, we note that the red shift of photoluminescence for the BPT-containing clusters (~15 nm) is less and almost half compared to that of BINAS-containing clusters (~30 nm), even though both the ligands are bidentate in nature. Furthermore, it is interesting to note that the red shift for the clusters containing 5–7 BPT ligands (see Figures S5 and S26) is less compared to that for the clusters with 4–7 BINAS ligands (see Figures 2D, S3D, and 10). However, there is no gradual increase in the red shift for these clusters as a function of the number of BINAS and BPT ligands in them. This can be due to the fact that all of the binaphthyl or biphenyl tail groups may not be able to adopt a favorable (planar) arrangement on clusters. Hence, an increasing conjugation of the π electrons (resulting in an increased red shift) with increasing number of BINAS or BPT ligands may not be possible. These observations suggest that the conjugation effects indeed play a role in the observed red shift of the luminescence; however, the conjugation alone cannot be the reason for the red shift of absorption and emission bands and that both of these effects are contributing to the observed changes in the absorption and emission features of BINAS-containing clusters. As the cluster $Ag_{24}Au_1(S\text{-BINAS})_4(DMBT)_{10}$ represents the $Ag_{24}Au_1(R/S\text{-BINAS})_x(DMBT)_{18-2x}$ clusters in general, as mentioned previously, and DFT calculations show the involvement of binaphthyl groups in the MOs (see Table S1 and Figure S19) associated with the low-energy transitions, we think that the changes in absorption and emission bands could be due to the incorporation of the BINAS ligands and associated effects mentioned above. However, it is difficult to disentangle the contributions of the structural distortion and conjugation in greater detail from the present study.

The CD spectroscopic measurements presented above reveal that the incorporation of BINAS induces chiroptical signatures in these clusters. Therefore, it is worthwhile to check whether this induced chirality has any effect on the luminescence of these clusters. In order to test this, we carried out CPL spectroscopy on groups I–IV. Our measurements show that even though there are well-defined signatures in the CD spectra, these clusters exhibit very weak CPL activity, as shown in Figures S28 and S29. Due to the weak signal, averaged spectra are presented for each sample. Due to instrumental limitations, the fluorescence maximum could not be reached, so we can just say that within the observed range one may estimate a value of 1.5×10^{-4} for the g_{lum} ratio, whereas g_{abs} for the lowest-energy band is about $5–8 \times 10^{-4}$. We note that the clusters with *R*-BINAS and *S*-BINAS exhibit positive and negative CPL bands, respectively, which is in accordance with the signs of their CD bands (see Figures 4 and 5). Furthermore, we note that the group IV (*i.e.*, $Ag_{24}Au_1(R/S\text{-BINAS})_x(DMBT)_{18-2x}$ clusters with 4–7 BINAS ligands) do not exhibit any CPL bands within our detection limit (see Supplementary Note 1): this sample exhibits distinct UV/vis and CD bands at 475 and 347 nm (see Figure 3, traces d and d′ in Figure 4 and Figure S13) but no CD signal at 645 nm (in the same experimental conditions of the other samples). A further discussion on the origin of luminescence in these clusters is presented in the next section in light of DFT calculations.

Discussion on the Origin of Chiroptical Features and Photoluminescence in $Ag_{24}Au_1(SR)_{18}$ and $Ag_{24}Au_1(S\text{-BINAS})_4(DMBT)_{10}$. The $Ag_{24}Au_1(SR)_{18}$ is structurally analogous to $Au_{25}(SR)_{18}$ and $Ag_{25}(SR)_{18}$. These clusters share common structural features, that is, an M_{13} icosahedral core and six $M_2(SR)_3$ staple motifs (M = Ag/Au).[2,3,36,48] All three clusters (anions) are superatoms[49,50] with eight free valence electrons contributed from the metal atoms of their icosahedral cores and an overall negative charge. Considering the electronic absorption spectra, previous theoretical calculations suggest that the low-energy absorption band of these clusters (at ~690 nm for $Au_{25}(SR)_{18}$, ~680 nm for $Ag_{25}(SR)_{18}$, and ~619 nm for $Ag_{24}Au_1(SR)_{18}$) originates from the intraband transitions involving superatomic orbitals derived from the metal atoms of their M_{13} icosahedral core.[13,19] The electronic absorption bands at higher energies are due to various transitions involving the molecular orbitals with significant contributions from the

sulfur atoms and the tail groups of their ligands.[19] However, there are contradicting conclusions on the nature of the transitions responsible for their photoluminescence. As mentioned previously, experiments suggest that the photoluminescence in $Ag_{24}Au_1(DMBT)_{18}$ is due to the charge transfer processes involving the ligands,[18] whereas theoretical calculations by Aikens *et al.* suggest that the photoluminescence in $M_{25}(SR)_{18}$ (M = Ag/Au) clusters is due to the transitions involving the icosahedral core-based superatomic orbitals and that the contribution of the ligands and the metal atoms in the staple motifs is not significant in these transitions.[19] We solve this discrepancy by noting that the orbital analysis in that work was limited to SH groups, instead of DMBT ligands, whose aromatic ligands are expected to behave quite differently with respect to the much simpler SH, due to coupling *via* conjugation between the ligand and the metal core.[51] Based on our experimental observations and DFT calculations presented above, we now discuss the nature of the electronic transitions responsible for the photoluminescence of $Ag_{24}Au_1(DMBT)_{18}$ and $Ag_{24}Au_1(R/S\text{-BINAS})_x(DMBT)_{18-2x}$ clusters.

UV/vis spectra show that the absorption band at around 619 nm for $Ag_{24}Au_1(DMBT)_{18}$ undergoes systematic changes with increasing number of incorporated BINAS ligands. The group of clusters I, II, and III exhibit strong absorption bands in the UV/vis spectra and corresponding CD bands (see Figures 3, 4, and S6). Similarly, the luminescence maximum of groups I−IV is red-shifted with regard to that of $Ag_{24}Au_1(DMBT)_{18}$. Interestingly, even though the group IV $Ag_{24}Au_1(R\text{-BINAS})_x(DMBT)_{18-2x}$ clusters with 4−7 BINAS ligands exhibit a band in the UV/vis spectra at around 590 nm (Figure 3), this sample does not have the corresponding CD band (*i.e.*, there is no band in traces d and d′ at low energies, corresponding to the ones at 645 nm for groups I−III; see Figure 4). Paralleling the UV/vis and the CD responses, no CPL was observed for this sample (see Supplementary Note 1), whereas weak CPL was observed for the other three $Ag_{24}Au_1(R\text{-BINAS})_x(DMBT)_{18-2x}$ clusters containing lower numbers of BINAS ligands.

In order to understand the origin of luminescence and CPL in $Ag_{24}Au_1(R/S\text{-BINAS})_x(DMBT)_{18-2x}$ clusters, the nature of molecular orbitals (in terms of the contributions of the metal atoms, in the cores and the staples, and ligands) involved in these transitions are to be considered. The MO diagram, based on the calculations on the model system, $[Ag_{24}Au_1(S\text{-BINAS})_4(DMBT)_{10}]^-$, shows the leading contributions to the two lowest transitions at 795 nm (1.56 eV) and 632 nm (1.96 eV) for the geometry "best 1", as shown in Figure 8. The DFT calculations show that the calculated CD band at around 632 nm is due to HOMO−1 → LUMO+2 and LUMO+3 transitions. Furthermore, the analysis of the molecular orbitals (see Figure 8, Figure S19, and Table S1) shows that the occupied molecular orbital (*i.e.*, HOMO−1) for this transition is mostly localized on the metal−ligand staple motifs (with noticeable Ag and S contributions), and the excited MOs (*i.e.*, LUMO+2 and LUMO +3) are mostly localized on the ligand's carbon atoms, giving an appreciable CD signal. However, this level of DFT predicts low-energy bands (estimated to lie around 795 nm by our TDDFT but arguably in the tail of the 632 nm at the experimental level), associated with HOMO−1, HOMO−2 → LUMO, LUMO+1 transitions, which are dark in the CD spectrum. For the photoluminescence and CPL activity, we can then argue that they should be assigned to an excitation transfer from the 632 nm band to its neighboring low-energy excited states (LUMO/LUMO+1, those calculated by TDDFT around 795 nm), which should become the leading decay channel in luminescence and CPL. This suggests that the luminescence and CPL activity of $Ag_{24}Au_1(R/S\text{-BINAS})_x(DMBT)_{18-2x}$ clusters could arise from these low-lying excited states (LUMO and LUMO+1) where the contribution of the ligand's tail groups (C and H atoms) is lower compared to that in the higher excited states (LUMO+2 and LUMO+3) (see Figure 8). However, the contributions from of the whole ligand (all of the atoms, S, C, and H) are important, as indicated by the red shift in the luminescence maximum when the DMBT ligands are exchanged with BPT and BINAS ligand which have larger aromatic tail groups. The red shift could be due to the fact that corresponding molecular orbitals have lower energies in BPT and BINAS compared to that in DMBT. The nature of the LUMO and LUMO+1 also explains the low values of circularly polarized luminescence, as chiral bands are lost in the evolution of these excited states in which electrons reside in the less chiral $Ag_{24}Au_1S_{18}$ framework of the cluster. As the CD response of the bands predicted at 795 nm is very weak, we expect a very low CPL signal, in agreement with experiment. This assignment is strongly corroborated by the red shift of ≈30 nm in the calculated photoabsorption band at 795 nm in going from $Ag_{24}Au_1(DMBT)_{18}$ to $Ag_{24}Au_1(R/S\text{-BINAS})_x(DMBT)_{18-2x}$ (see Figure 7, left panel), which matches a corresponding red shift as measured in the experimental photoluminescence spectra. In Table S2, an analysis of the calculated spectral bands at 765 and 590 nm of the parent, achiral cluster, $Ag_{24}Au_1(DMBT)_{18}$ is shown with the orbitals involved (see Figure S30). Their nature is similar as found in the $[Ag_{24}Au_1(S\text{-BINAS})_4(DMBT)_{10}]^-$ cluster, and the only difference is the absence of the ligand's aromatic ring participation at the 590 nm transition. Therefore, theoretical results and the correlations between the observed UV/vis, CD, luminescence, and CPL bands of groups I−IV with that of the $Ag_{24}Au_1(DMBT)_{18}$ confirm that the luminescence in these clusters occurs due to the transitions involving the whole $Ag_{24}Au_1S_{18}$ framework and not merely from the icosahedral $Ag_{12}Au_1$ core.

CONCLUSIONS

In summary, we presented an experimental approach utilizing chiroptical spectroscopic techniques to probe the origin of electronic transitions responsible for the photoluminescence of an atomically precise noble metal cluster, namely, $Ag_{24}Au_1(DMBT)_{18}$, and chiroptical responses in its chirally functionalized derivatives. To the best of our knowledge, a combination of the chiroptical and luminescence spectroscopies to understand the nature of electronic transitions has not been applied in such molecule-like metal clusters. In order to enable the use of chiroptical techniques, a chiral ligand, *R*/*S*-1,1′-[binaphthalene]-2,2′-dithiol (*R*/*S*-BINAS) was incorporated into $Ag_{24}Au_1(DMBT)_{18}$, and a series of clusters of the general formula $Ag_{24}Au_1(R/S\text{-BINAS})_x(DMBT)_{18-2x}$, with x = 1−7, were synthesized without altering the overall structure and composition. The effect of BINAS on the UV/vis, CD, luminescence, and CPL bands of these clusters was systematically analyzed, which reveals an unexpected transition of the low-energy electronic excitations from achiral to chiral and back to achiral from $Ag_{24}Au_1(DMBT)_{18}$ to $Ag_{24}Au_1(R/S\text{-BINAS})_x(DMBT)_{18-2x}$ by increasing the number of incorporated BINAS ligands. Our chiroptical spectroscopic measurements, in conjunction with DFT calculations, suggest that the photoluminescence in $Ag_{24}Au_1(DMBT)_{18}$ and its chirally functionalized derivatives originates from the transitions involving the

whole $Ag_{24}Au_1S_{18}$ framework and not merely from the icosahedral $Ag_{12}Au_1$ core, with an important contribution of conjugation effects with aromatic tails of the ligands.[51] These results show that the photoluminescence in these cluster systems cannot be solely attributed to any one of the structural components, that is, the metal core or the protecting metal−ligand oligomeric units, but rather to their interaction and that the ligand shell plays a crucial role.[52] Our work demonstrates that chiroptical spectroscopic techniques such as circular dichroism and circularly polarized luminescence represent useful tools to understand the nature of electronic transitions in ligand-protected metal clusters and that this approach can be utilized for gaining deeper insights into the structure−property relationships of the electronic transitions of such molecule-like cluster systems.

EXPERIMENTAL SECTION

Materials Used. Silver nitrate ($AgNO_3$), 2,4-dimethylbenzene thiol (DMBT), tetraphenylphosphonium bromide (PPh_4Br), and sodium borohydride ($NaBH_4$) were purchased form Sigma-Aldrich. Chloro(triphenylphosphine)gold(I) ($AuClPPh_3$) was purchased from Acros Chemicals. All solvents used, dichloromethane (DCM), methanol, *etc.*, were of analytical grade and used without further purification. 1,1-[binaphthalene]-2,2-dithiol (BINAS) and 1,1′-biphenyldithiol (BPT) were synthesized by adopting the method reported previously.[53−55] Bio Beads SX-1 (Bio-Rad) for column size-exclusion chromatography was purchased from Bio-Rad Companies, USA.

Instrumentation. Ultraviolet−visible spectra were recorded on a Varian Cary 50 spectrophotometer using a quartz cuvette with a 10 mm path length. CD spectra were recorded on a JASCO J-815SE CD spectrometer using a quartz cuvette with a 2 mm path length. All CD and UV/vis measurements were carried out using DCM as the solvent.

Electrospray ionization mass spectra were measured on a QSTAR pulsar *i* (AB Sciex) using a quadrupole and time-of-flight analyzers. The spectra were measured in the mass range of m/z 500−12,000 in the negative ion mode. Further details of the instrumental parameters used for the measurements are provided in the Supporting Information.

Emission spectra were measured on a Fluorolog-3 fluorescence spectrometer (Horiba JobinYvon) equipped with a liquid nitrogen-cooled NIR photomultiplier tube with an extended detection capability in the visible region (R5509-73, Hamamatsu). The measurements were carried out using a quartz cuvette with a 1 cm path length. DCM was used as solvent for all of the measurements. All of the emission spectra were collected at an excitation wavelength of 467 nm (unless otherwise stated) with an excitation monochromator slit of 5 nm and an emission slit of 2 nm.

Circularly polarized luminescence spectra were measured using a home-built spectrometer (allowing to simultaneously record also fluorescence spectra).[56] DCM was used as solvent for all of the measurements. The same solutions employed for CD measurements were used in a 10 mm × 2 mm fluorescence quartz cell. Excitation radiation (470 nm wavelength) was brought to the sample through an optical fiber from a Jasco FP8200 fluorimeter. Thirty scans were accumulated for each spectrum, with the following conditions: incident bandwidth of 20 nm, emission band pass of approximately 10 nm, and scan speed of 0.5 nm/s. The signal is very noisy due both to low fluorescence of samples and to low sensitivity of the instrument in the spectroscopic region of interest; for this reason, the spectra are plotted after an "adjacent average" over 100 points (data pitch 0.25 nm). The original spectra are reported in Figure S29.

Synthesis of $[Ag_{24}Au_1(DMBT)_{18}][PPh_4]$. $[Ag_{24}Au_1(DMBT)_{18}][PPh_4]$ was synthesized by the reaction of $[Ag_{25}(DMBT)_{18}][PPh_4]$ with $AuClPPh_3$ by adopting a reported procedure[36] with slight modifications. $[Ag_{25}(DMBT)_{18}][PPh_4]$ was synthesized by adopting a reported procedure.[48] To synthesize $[Ag_{24}Au_1(DMBT)_{18}][PPh_4]$, 16 mg of $[Ag_{25}(DMBT)_{18}][PPh_4]$ was dissolved in 5 mL of DCM. Two hundred microliters of $AuClPPh_3$ solution (4.2 mg in 500 μL of DCM) was then added to it. The reaction mixture was gently shaken by hand and kept undisturbed for about 2 h. The color of the solution changed from dark brown to dark green during this time interval, indicating the formation of $[Ag_{24}Au_1(DMBT)_{18}][PPh_4]$. Formation of the alloy cluster was confirmed using UV/vis spectroscopy. The reaction mixture was then centrifuged at a speed of ∼ 10000 rpm for about ten minutes in order to remove any insoluble materials formed (AgCl, for example) and the supernatant DCM solution was collected and dried using a rotary evaporator. Then the reaction mixture was passed through a size exclusion chromatographic column using DCM as the eluting solvent. The pure $[Ag_{24}Au_1(DMBT)_{18}][PPh_4]$ thus obtained was dried using rotary evaporation.

Synthesis of $[Ag_{24}Au_1(R/S\text{-BINAS})_x(DMBT)_{18-2x}][PPh_4]$. These clusters were synthesized through a ligand exchange reaction of $[Ag_{24}Au_1(DMBT)_{18}][PPh_4]$ with *R*/*S*-BINAS. The number of BINAS ligands incorporated (*i.e.*, x) in the general molecular formula, $Ag_{24}Au_1(R/S\text{-BINAS})_x(DMBT)_{18-2x}$, is controlled by varying the $Ag_{24}Au_1(DMBT)_{18}$/BINAS molar ratios. The groups of $Ag_{24}Au_1(R/S\text{-BINAS})_x(DMBT)_{18-2x}$ clusters with varying numbers of BINAS in them, I (x = 0−3), II (x = 2−5), and III (x = 3−5), were synthesized at $Ag_{24}Au_1(DMBT)_{18}$/BINAS molar ratios of 0.5:1.0, 0.25:1.0, and 0.1:1.0, respectively. The $Ag_{24}Au_1(S\text{-BINAS})_x(DMBT)_{18-2x}$ clusters of group IV (x = 4−7) were synthesized at a $Ag_{24}Au_1(DMBT)_{18}$/*S*-BINAS molar ratio of 0.01:1.0. The $Ag_{24}Au_1(R\text{-BINAS})_x(DMBT)_{18-2x}$ of group IV was synthesized by furthering the ligand exchange of the corresponding group II, wherein x = 2−5. For the synthesis of $Ag_{24}Au_1(R/S\text{-BINAS})_x(DMBT)_{18-2x}$, typically, ∼2.5 mg of $[Ag_{24}Au_1(DMBT)_{18}][PPh_4]$ was dissolved in 1 mL of DCM. Then, various volumes of *R*/*S*-BINAS solution (2 mg in 100 μL of DCM) was added to it. The mixture was then shaken gently by hand and kept undisturbed for about 1.5 h at room temperature. The reaction mixture was then purified by size exclusion chromatography using DCM as the eluting solvent.

Synthesis of $[Ag_{24}Au_1(BPT)_x(DMBT)_{18-2x}][PPh_4]$. These clusters were synthesized through a ligand exchange reaction of $[Ag_{24}Au_1(DMBT)_{18}][PPh_4]$ with BPT. Typically, 2.0 mg of $[Ag_{24}Au_1(DMBT)_{18}][PPh_4]$ was dissolved in 1 mL of DCM. Then, various volumes of BPT solution (2 mg of BPT in 100 μL of DCM) were added to it. The mixture was then shaken gently by hand and kept undisturbed for about 1 h at room temperature. The reaction mixture was then purified by size exclusion chromatography using DCM as the eluting solvent.

ASSOCIATED CONTENT

Supporting Information

The Supporting Information is available free of charge at https://pubs.acs.org/doi/10.1021/acsnano.0c01183.

Parameters used for ESI MS measurements, computational details, additional mass spectrometry data, UV/vis spectroscopy data, CD, luminescence, CPL data, additional DFT results, energies and coordinates of $Ag_{24}Au_1(DMBT)_{18}$, all isomer structural models from the docking study (PDF)

AUTHOR INFORMATION

Corresponding Authors

Thomas Bürgi − *Département de Chimie Physique, Université de Genève, 1211 Geneva 4, Switzerland;* orcid.org/0000-0003-0906-082X; Email: thomas.buergi@unige.ch

Kumaranchira Ramankutty Krishnadas − *Département de Chimie Physique, Université de Genève, 1211 Geneva 4, Switzerland*; Email: krishnadas.kumaranchiraramankutty@unige.ch

Mauro Stener − *Dipartimento di Scienze Chimiche e Farmaceutiche, Università degli Studi di Trieste, 34127 Trieste, Italy;* orcid.org/0000-0003-3700-7903; Email: stener@units.it

Authors

Luca Sementa − *CNR-ICCOM & IPCF, Consiglio Nazionale delle Ricerche, 56124 Pisa, Italy*

Marco Medves − *Dipartimento di Scienze Chimiche e Farmaceutiche, Università degli Studi di Trieste, 34127 Trieste, Italy*

Alessandro Fortunelli − *CNR-ICCOM & IPCF, Consiglio Nazionale delle Ricerche, 56124 Pisa, Italy;* orcid.org/0000-0001-5337-4450

Alexandre Fürstenberg − *Département de Chimie Analytique et Minérale, Université de Genève, 1211 Geneva 4, Switzerland;* orcid.org/0000-0002-6227-3122

Giovanna Longhi − *Dipartimento di Medicina Molecolare e Traslazionale, Università di Brescia, 25123 Brescia, Italy;* orcid.org/0000-0002-0011-5946

Complete contact information is available at: https://pubs.acs.org/10.1021/acsnano.0c01183

Notes

The authors declare no competing financial interest.

ACKNOWLEDGMENTS

Financial support from the University of Geneva and the Swiss National Science Foundation (Grant No. 200020_172511) is kindly acknowledged. We also acknowledge the support from the MZ 2.0 mass spectrometry core facility at the Faculty of Sciences, University of Geneva. This work was supported by Stiftung Beneficentia and by Finanziamento per la Ricerca di Ateneo (FRA) of the Università degli Studi di Trieste. Computational resources from the Cineca Supercomputing Center is gratefully acknowledged (Project CHROMPC). We thank Dr. Arnulf Rosspeintner for fruitful discussions.

REFERENCES

(1) Jadzinsky, P. D.; Calero, G.; Ackerson, C. J.; Bushnell, D. A.; Kornberg, R. D. Structure of a Thiol Monolayer-Protected Gold Nanoparticle at 1.1 Å Resolution. *Science* **2007**, *318*, 430−433.

(2) Akola, J.; Walter, M.; Whetten, R. L.; Häkkinen, H.; Grönbeck, H. On the Structure of Thiolate-Protected Au_{25}. *J. Am. Chem. Soc.* **2008**, *130*, 3756−3757.

(3) Heaven, M. W.; Dass, A.; White, P. S.; Holt, K. M.; Murray, R. W. Crystal Structure of the Gold Nanoparticle $[N(C_8H_{17})_4][Au_{25}(SCH_2CH_2Ph)_{18}]$. *J. Am. Chem. Soc.* **2008**, *130*, 3754−3755.

(4) Lopez-Acevedo, O.; Tsunoyama, H.; Tsukuda, T.; Hakkinen, H.; Aikens, C. M. Chirality and Electronic Structure of the Thiolate-Protected Au_{38} Nanocluster. *J. Am. Chem. Soc.* **2010**, *132*, 8210−8218.

(5) Qian, H.; Eckenhoff, W. T.; Zhu, Y.; Pintauer, T.; Jin, R. Total Structure Determination of Thiolate-Protected Au_{38} Nanoparticles. *J. Am. Chem. Soc.* **2010**, *132*, 8280−8281.

(6) Dolamic, I.; Knoppe, S.; Dass, A.; Bürgi, T. First Enantioseparation and Circular Dichroism Spectra of Au_{38} Clusters Protected by Achiral Ligands. *Nat. Commun.* **2012**, *3*, 798.

(7) Desireddy, A.; Conn, B. E.; Guo, J.; Yoon, B.; Barnett, R. N.; Monahan, B. M.; Kirschbaum, K.; Griffith, W. P.; Whetten, R. L.; Landman, U.; Bigioni, T. P. Ultrastable Silver Nanoparticles. *Nature* **2013**, *501*, 399−402.

(8) Yang, H.; Wang, Y.; Huang, H.; Gell, L.; Lehtovaara, L.; Malola, S.; Hakkinen, H.; Zheng, N. All-Thiol-Stabilized Ag_{44} And $Au_{12}Ag_{32}$ Nanoparticles with Single-Crystal Structures. *Nat. Commun.* **2013**, *4*, 2422.

(9) Harkness, K. M.; Tang, Y.; Dass, A.; Pan, J.; Kothalawala, N.; Reddy, V. J.; Cliffel, D. E.; Demeler, B.; Stellacci, F.; Bakr, O. M.; McLean, J. A. $Ag_{44}(SR)_{30}^{4-}$: A Silver-Thiolate Superatom Complex. *Nanoscale* **2012**, *4*, 4269−4274.

(10) Chakraborty, I.; Pradeep, T. Atomically Precise Clusters of Noble Metals: Emerging Link between Atoms and Nanoparticles. *Chem. Rev.* **2017**, *117*, 8208−8271.

(11) Jin, R.; Zeng, C.; Zhou, M.; Chen, Y. Atomically Precise Colloidal Metal Nanoclusters and Nanoparticles: Fundamentals and Opportunities. *Chem. Rev.* **2016**, *116*, 10346−10413.

(12) Krishnadas, K. R.; Baksi, A.; Ghosh, A.; Natarajan, G.; Pradeep, T. Structure-Conserving Spontaneous Transformations between Nanoparticles. *Nat. Commun.* **2016**, *7*, 13447.

(13) Zhu, M.; Aikens, C. M.; Hollander, F. J.; Schatz, G. C.; Jin, R. Correlating the Crystal Structure of a Thiol-Protected Au_{25} Cluster and Optical Properties. *J. Am. Chem. Soc.* **2008**, *130*, 5883−5885.

(14) Aikens, C. M. Origin of Discrete Optical Absorption Spectra of $M_{25}(SH)_{18}^-$ Nanoparticles (M = Au, Ag). *J. Phys. Chem. C* **2008**, *112*, 19797−19800.

(15) Fernando, A.; Weerawardene, K. L. D. M.; Karimova, N. V.; Aikens, C. M. Quantum Mechanical Studies of Large Metal, Metal Oxide, and Metal Chalcogenide Nanoparticles and Clusters. *Chem. Rev.* **2015**, *115*, 6112−6216.

(16) Xie, J.; Zheng, Y.; Ying, J. Y. Highly Selective and Ultrasensitive Detection of Hg^{2+}Based on Fluorescence Quenching of Au Nanoclusters by Hg^{2+}-Au^+ Interactions. *Chem. Commun.* **2010**, *46*, 961−963.

(17) Wu, Z.; Jin, R. On the Ligand's Role in the Fluorescence of Gold Nanoclusters. *Nano Lett.* **2010**, *10*, 2568−2573.

(18) Liu, X.; Yuan, J.; Yao, C.; Chen, J.; Li, L.; Bao, X.; Yang, J.; Wu, Z. Crystal and Solution Photoluminescence of $MAg_{24}(SR)_{18}$ (M = Ag/Pd/Pt/Au) Nanoclusters and Some Implications for the Photoluminescence Mechanisms. *J. Phys. Chem. C* **2017**, *121*, 13848−13853.

(19) Weerawardene, K. L. D. M.; Aikens, C. M. Origin of Photoluminescence of $Ag_{25}(SR)_{18}^-$ Nanoparticles: Ligand and Doping Effect. *J. Phys. Chem. C* **2018**, *122*, 2440−2447.

(20) Mustalahti, M.; Myllyperkio, P.; Malola, S.; Lahtinen, T.; Salorinne, K.; Koivisto, J.; Hakkinen, H.; Pettersson, M. Molecule-Like Photodynamics of $Au_{102}(pMBA)_{44}$ Nanocluster. *ACS Nano* **2015**, *9*, 2328−2335.

(21) Mustalahti, S.; Myllyperkiö, P.; Lahtinen, T.; Salorinne, K.; Malola, S.; Koivisto, J.; Hakkinen, H.; Pettersson, M. Ultrafast Electronic Relaxation and Vibrational Cooling Dynamics of $Au_{144}(SC_2H_4Ph)_{60}$ Nanocluster Probed by Transient Mid-IR Spectroscopy. *J. Phys. Chem. C* **2014**, *118*, 18233−18239.

(22) Green, T. D.; Yi, C.; Zeng, C.; Jin, R.; McGill, S.; Knappenberger, K. L., Jr. Temperature-Dependent Photoluminescence of Structurally-Precise Quantum-Confined $Au_{25}(SC_8H_9)_{18}$ and $Au_{38}(SC_{12}H_{25})_{24}$ Metal Nanoparticles. *J. Phys. Chem. A* **2014**, *118*, 10611−10621.

(23) Li, Q.; Zhou, M.; So, W. Y.; Huang, J.; Li, M.; Kauffman, D. R.; Cotlet, M.; Higaki, T.; Peteanu, L. A.; Shao, Z.; Jin, R. A Mono-Cuboctahedral Series of Gold Nanoclusters: Photoluminescence Origin, Large Enhancement, Wide Tunability, and Structure-Property Correlation. *J. Am. Chem. Soc.* **2019**, *141*, 5314−5325.

(24) Riehl, J. P.; Richardson, F. S. Circularly Polarized Luminescence Spectroscopy. *Chem. Rev.* **1986**, *86*, 1−16.

(25) Kumar, J.; Nakashima, T.; Kawai, T. Circularly Polarized Luminescence in Chiral Molecules and Supramolecular Assemblies. *J. Phys. Chem. Lett.* **2015**, *6*, 3445−3452.

(26) Longhi, G.; Castiglioni, E.; Koshoubu, J.; Mazzeo, G.; Abbate, S. Circularly Polarized Luminescence: A Review of Experimental and Theoretical Aspects. *Chirality* **2016**, *28*, 696−707.

(27) Schaaff, T. G.; Whetten, R. L. Giant Gold-Glutathione Cluster Compounds: Intense Optical Activity in Metal-Based Transitions. *J. Phys. Chem. B* **2000**, *104*, 2630−2641.

(28) Zhu, M.; Qian, H.; Meng, X.; Jin, S.; Wu, Z.; Jin, R. Chiral Au_{25}Nanospheres and Nanorods: Synthesis and Insight into the Origin of Chirality. *Nano Lett.* **2011**, *11*, 3963−3969.

(29) Sanchez-Castillo, A.; Noguez, C.; Garzon, I. L. On the Origin of the Optical Activity Displayed by Chiral-Ligand-Protected Metallic Nanoclusters. *J. Am. Chem. Soc.* **2010**, *132*, 1504−1505.

(30) Noguez, C.; Garzon, I. L. Optically Active Metal Nanoparticles. *Chem. Soc. Rev.* **2009**, *38*, 757−771.

(31) Zeng, C.; Chen, C.; Liu, C.; Nobusada, K.; Rosi, N. L.; Jin, R. Gold Tetrahedra Coil Up: Kekulé-Like and Double Helical Superstructures. *Sci. Adv.* **2015**, *1*, No. e1500425.
(32) Pelayo, J. J.; Whetten, R. L.; Garzon, I. L. Geometric Quantification of Chirality in Ligand-Protected Metal Clusters. *J. Phys. Chem. C* **2015**, *119*, 28666−28678.
(33) Tanaka, H.; Kato, Y.; Fujiki, M.; Inoue, Y.; Mori, T. Combined Experimental and Theoretical Study on Circular Dichroism and Circularly Polarized Luminescence of Configurationally Robust D_3-Symmetric Triple Pentahelicene. *J. Phys. Chem. A* **2018**, *122*, 7378−7384.
(34) Longhi, G.; Castiglioni, E.; Abbate, S.; Lebon, F.; Lightner, D. A. Experimental and Calculated CPL Spectra and Related Spectroscopic Data of Camphor and Other Simple Chiral Bicyclic Ketones. *Chirality* **2013**, *25*, 589−599.
(35) Mori, T. Frontiers of Circularly Polarized Luminescence Chemistry of Isolated Small Organic Molecules. *Circularly Polarized Luminescence of Isolated Small Organic Molecules*, 1st ed.; Springer: Singapore, 2020; pp 1−10.
(36) Bootharaju, M. S.; Joshi, C. P.; Parida, M. R.; Mohammed, O. F.; Bakr, O. M. Templated Atom-Precise Galvanic Synthesis and Structure Elucidation of a $[Ag_{24}Au(SR)_{18}]^-$ Nanocluster. *Angew. Chem.* **2016**, *128*, 934−938.
(37) Knoppe, S.; Bürgi, T. The Fate of $Au_{25}(SR)_{18}$ Clusters upon Ligand Exchange with Binaphthyl-Dithiol: Interstaple Binding *vs* Decomposition. *Phys. Chem. Chem. Phys.* **2013**, *15*, 15816−15820.
(38) Sels, A.; Barrabés, N.; Knoppe, S.; Bürgi, T. Isolation of Atomically Precise Mixed Ligand Shell $PdAu_{24}$ Clusters. *Nanoscale* **2016**, *8*, 11130−11135.
(39) Jupally, V. R.; Kota, R.; Dornshuld, E. V.; Mattern, D. L.; Tschumper, G. S.; Jiang, D.-e.; Dass, A. Interstaple Dithiol Cross-Linking in $Au_{25}(SR)_{18}$Nanomolecules: A Combined Mass Spectrometric and Computational Study. *J. Am. Chem. Soc.* **2011**, *133*, 20258−20266.
(40) Molina, B.; Sánchez-Castillo, A.; Knoppe, S.; Garzón, I. L.; Bürgi, T.; Tlahuice-Flores, A. Structures and Chiroptical Properties of the BINAS-Monosubstituted $Au_{38}(SCH3)_{24}$ Cluster. *Nanoscale* **2013**, *5*, 10956−10962.
(41) Baseggio, O.; Fronzoni, G.; Stener, M. A New Time Dependent Density Functional Algorithm for Large Systems and Plasmons in Metal Clusters. *J. Chem. Phys.* **2015**, *143*, 024106.
(42) Baseggio, O.; Toffoli, D.; Fronzoni, G.; Stener, M.; Sementa, L.; Fortunelli, A. Extension of the Time Dependent Density Functional Complex Polarizability Algorithm to Circular Dichroism: Implementation and Applications to Ag_8 and $Au_{38}(SC_2H_4C_6H_5)_{24}$. *J. Phys. Chem. C* **2016**, *120*, 24335−24345.
(43) Baseggio, O.; De Vetta, M.; Fronzoni, G.; Toffoli, D.; Stener, M.; Sementa, L.; Fortunelli, A. Time-Dependent Density-Functional Study of the Photoabsorption Spectrum of $Au_{25}(SC_2H_4C_6H_5)_{18}$ Anion: Validation of the Computational Protocol. *Int. J. Quantum Chem.* **2018**, *118*, No. e25769.
(44) Becke, A. D. Density-Functional Thermochemistry. III. The Role of Exact Exchange. *J. Chem. Phys.* **1993**, *98*, 5648−5652.
(45) Medves, M.; Sementa, L.; Toffoli, D.; Fronzoni, G.; Fortunelli; Stener, M. An Efficient Hybrid Scheme for Time Dependent Density Functional Theory. *J. Chem. Phys.* **2020**, *152*, 184104.
(46) Toffoli, D.; Baseggio, O.; Fronzoni, G.; Stener, M.; Fortunelli, A.; Sementa, L. Pd Doping, Conformational, and Charge Effects on the Dichroic Response of a Monolayer Protected $Au_{38}(SR)_{24}$ Nanocluster. *Phys. Chem. Chem. Phys.* **2019**, *21*, 3585−3596.
(47) Chang, L.; Baseggio, O.; Sementa, L.; Cheng, D.; Fronzoni, G.; Toffoli, D.; Aprà, E.; Stener, M.; Fortunelli, A. Individual Component Map of Rotatory Strength and Rotatory Strength Density Plots as Analysis Tools of Circular Dichroism Spectra of Complex Systems. *J. Chem. Theory Comput.* **2018**, *14*, 3703−3714.
(48) Joshi, C. P.; Bootharaju, M. S.; Alhilaly, M. J.; Bakr, O. M. $[Ag_{25}(SR)_{18}]^-$: The "Golden" Silver Nanoparticle. *J. Am. Chem. Soc.* **2015**, *137*, 11578−11581.
(49) Walter, M.; Akola, J.; Lopez-Acevedo, O.; Jadzinsky, P. D.; Calero, G.; Ackerson, C. J.; Whetten, R. L.; Grönbeck, H.; Häkkinen, H. A Unified View of Ligand-Protected Gold Clusters as Superatom Complexes. *Proc. Natl. Acad. Sci. U. S. A.* **2008**, *105*, 9157−9162.
(50) Häkkinen, H. Atomic and Electronic Structure of Gold Clusters: Understanding Flakes, Cages and Superatoms from Simple Concepts. *Chem. Soc. Rev.* **2008**, *37*, 1847−1859.
(51) Sementa, L.; Barcaro, G.; Dass, A.; Stener, M.; Fortunelli, A. Designing Ligand-Enhanced Optical Absorption of Thiolated Gold Nanoclusters. *Chem. Commun.* **2015**, *51*, 7935−7938.
(52) Rambukwella, M.; Sakthivel, N. A.; Delcamp, J. H.; Sementa, L.; Fortunelli, A.; Dass, A. Ligand Structure Determines Nanoparticles' Atomic Structure, Metal-Ligand Interface and Properties. *Front. Chem.* **2018**, *6*, 330.
(53) Fabbri, D.; Delogu, G.; De Lucchi, O. Preparation of Enantiomerically Pure 1,1′-Binaphthalene-2,2′-Diol and 1,1′-Binaphthalene-2,2′-Dithiol. *J. Org. Chem.* **1993**, *58*, 1748−1750.
(54) He, H.; Chen, L.-Y.; Wong, W.-Y.; Chan, W.-H.; Lee, A. W. M. Practical Synthetic Approach to Chiral Sulfonimides (CSIs) - Chiral Brønsted Acids for Organocatalysis. *Eur. J. Org. Chem.* **2010**, *2010*, 4181−4184.
(55) Knoppe, S.; Azoulay, R.; Dass, A.; Bürgi, T. *In Situ* Reaction Monitoring Reveals a Diastereoselective Ligand Exchange Reaction between the Intrinsically Chiral $Au_{38}(SR)_{24}$ and Chiral Thiols. *J. Am. Chem. Soc.* **2012**, *134*, 20302−20305.
(56) Castiglioni, E.; Abbate, S.; Longhi, G. Revisiting with Updated Hardware an Old Spectroscopic Technique: Circularly Polarized Luminescence. *Appl. Spectrosc.* **2010**, *64*, 1416−1419.